ACS APPLIED MATERIALS & INTERFACES

Research Article

www.acsami.org

Magnetic Self-Assembled Zeolite Clusters for Sensitive Detection and Rapid Removal of Mercury(II)

Meili Yin,[†,‡] Zhenhua Li,[†,‡] Zhen Liu,[†,‡] Xinjian Yang,[†,‡] and Jinsong Ren*[,†]

[†]State Key Laboratory of Rare Earth Resources Utilization and Laboratory of Chemical Biology, Changchun Institute of Applied Chemistry, Chinese Academy of Sciences, Changchun, 130022, P. R. China

[‡]Graduate School of the Chinese Academy of Sciences, Beijing, 100039, P. R. China

ABSTRACT: We reported here the fabrication of a hierarchical mesoporous zeolite nanocomposite using 20 nm crystalline domins of zeolite L as building "bricks" by a simple and general one-step synthetic approach. By taking advantages of the large pore volumes, superparamagnetic iron oxide nanocrystals could be encapsulated into the nanocomposite conveniently for further facilitate separation and detection. In addition, by covalent coupling of fluorescent receptor (rhodamine-hydrazine), the combination of well-defined inorganic nanomaterials and organic receptors could be applied to selective detection of Hg^{2+}. Importantly, the unique adsorption capacity enabled by the hierarchical mesoporous zeolite and the efficient removal ability form complex multiphase systems by the magnetic characteristic made this multifunctional nanomaterial an excellent probe for detection, adsorption, and removal of Hg^{2+} from waste aqueous solution.

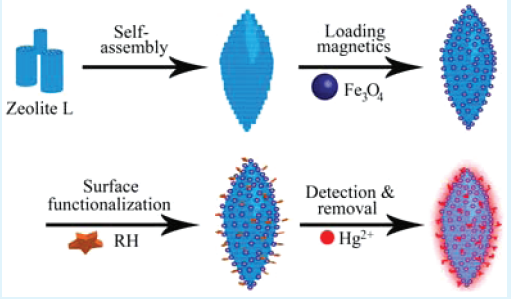

KEYWORDS: *mesoporous materials, rhodamine-hydrazine, magnetic nanoparticles, mercury(II), fluorescent probes*

1. INTRODUCTION

As an important number of the porous family materials, zeolite has been adopted in many industrial and biological applications, such as removal of toxic metal ions,[1−3] molecular separation and adsorption,[4−7] cell adhesion, and live system self-assembly.[8,9] However, the applications for catalysts involving large molecules, the adsorption and separation of biomolecules, removal of toxic metal ions, etc., are limited by the small pore sizes of zeolites. Recently, much research effort has been devoted to integrate mesopores into microporous zeolite by using different strategies, including steaming, acid (or base) etching, chemical treatment, zeolite seeds assembly, and template-assistant method.[10−17] These existing systems, although promising, are offset by the complex fabrication strategy by removal of templates, large consumption of acid/base and energy, low reactivity toward surface functionalization, macroscopic aggregation, amorphous morphological and structural features, as well as limited functional components. As a consequence, the development of novel mesoporous zeolite materials involving facile preparation, hierarchical pore size, optimal morphology, as well as rational surface-functionalization is still highly desirable. Although a hierarchical zeolite L network fabricated by a single step has been reported recently,[18] the synthesis of small and uniform size zeolites with hierarchical pores is still a challenge. More recently, Yin et al. reported the fabrication of novel porous nanostructured materials through the self-assembly of TiO_2 nanocrystal clusters.[19] The size and surface chemistry of the pores could be conveniently controlled by changing the properties of the building blocks during assembly. By taking the advantage of both the specific affinity offered by the metal oxide and the size exclusion mechanism enable by the mesoporous structure, selective enrichment of intact protein from complex biological samples could be realized. Inspired by this strategy, we reported here the fabrication of a hierarchical mesoporous zeolite nanocomposite using 20 nm crystalline domins of zeolite L as building "bricks" by a simple and general one-step synthetic approach. Importantly, the large pore volumes bring the convenience of encapsulating of multiple components into the clusters to further facilitate separation and detection. Herein, to the best of our knowledge, we demonstrated the first example of encapsulating of superparamagnetic iron oxide nanocrystals into the mesoporous zoelite network. In addition, by covalent coupling of fluorescent receptor, the combination of well-defined inorganic nanomaterials and organic receptors could play a pivotal role in the development of a new generation of hybrid nanomaterials with improved functionalities, which offer much promise in a wide range of biological, toxicological, and environmental applications. This work, using Hg^{2+} as a model example, we fabricated a new probe for sensitive detection and rapid removal of toxic ions from aqueous solution.

Recently, much attention has been given to the detection and removal of heavy metal ions from aqueous phases.[20−25] Zeolite is an ideal matrix to attract and hold heavy metals for its adsorption capacity originates from the open structure and a net negative charge in its framework.[26] The use of mesoporous

Received: October 31, 2011
Accepted: November 29, 2011
Published: November 29, 2011

organosilica or related nanomaterials for the fabrication of chemosensors through anchoring or grafting of organic groups in the nanochannels or surface is an active area of research.[20,27] Among the known heavy metal ions, Hg^{2+} is considered to be one of the most dangerous ions because it can accumulate in the human body and initiate a wide variety of symptoms, such as headache, edema, and enema, which have been reported after mercury exposure even at low concentrations.[28] Therefore, new materials are required to not only detect but also effectively remove mercury from environmental sources such as water. Although many sensors can effectively detect Hg^{2+} with fluorescence or color changes,[29] materials that can simultaneously detect and remove Hg^{2+} in aqueous solution are still very rare.[23−25] Here, as shown in Scheme 1, we report the fabrication of multifunctional magnetic mesoporous materials with magnetic nanoparticles doped in the zeolite nanonetworks and rhodamine-hydrazine (RH) immobilized at the surface. By taking advantage of the selectivity for Hg^{2+} offered by RH, the unique adsorption capacity enabled by the hierarchical mesoporous zeolite and the efficient removal ability form complex multiphase systems by the magnetic characteristic, this probe can be used for detection, adsorption, and removal of Hg^{2+} simultaneously.

Scheme 1. Schematic Representation of the Construction of Multifunctional Magnetic Mesoporous Rhodamine-Hydrazine Immobilized Zeolite Nanonetwoks and Its Application for Hg^{2+} Detection

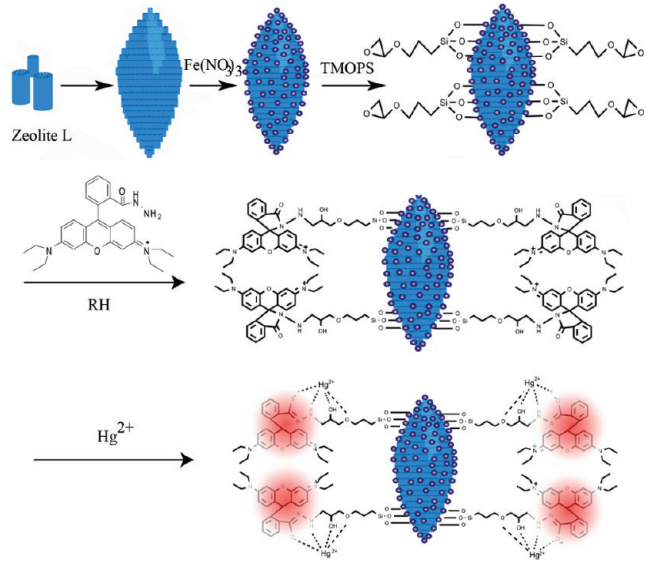

2. MATERIALS AND METHODS

2.1. Materials and Instrumentation. Rhodamine B (RB), trimethoxy[3-(oxiranylmethoxy)propyl]-silane, hydrazine hydrate (85%), toluene, and acetonitrile, $Fe(NO_3)_3$, were purchased from Sigma, $Al(OH)_3$, KOH, colloidal silica were purchased from Fluka. All chemicals were used as received from the suppliers without further purification. FTIR analys was carried out on a Bruker Vertex 70 FT-IR Spectrometer. X-ray measurements were performed on a Bruker D8 FOCUS Powder X-ray Diffractometer using Cu Ka radiation. SEM images were obtained with a Hitachi S-4800 FE-SEM. N_2 adsorption−desorption isotherms were recorded on a Micromeritics ASAP 2020 M automated sorption analyzer. Fluorescence spectra were recorded with a JASCO FP-6500 spectrofluorometer.

2.2. Synthesis of Mesoporous Zeolite Cluster (MZ). Solution A was prepared as follows: 0.624 g of $Al(OH)_3$ (Fluka, purum) was dissolved under reflux in a solution consisting of 4.489 g of KOH and 10.814 g of water until the mixture looks transparent. Solution B: 16.021 g of colloidal silica and 5.835 g of doubly distilled water were mixed and kept in an ultrasonic bath for at least 10 min. After being cooled to room temperature, solution A was added to solution B while stirring strongly. During vigorous stirring, this mixture turned into a thick opaque gel, which was then transferred into 50 mL autoclave, sealed, and hydrothermally treated at 160 °C for 20 h.

2.3. Synthesis of Magnetic Functionalized Zeolite (MMZ). $Fe(NO_3)_3{\cdot}9H_2O$ (0.72 g) was dissolved in 0.5 mL of acetonitrile. Zeolites were suspended in 5 mL of hexane. The $Fe(NO_3)_3$ solution was then added to the zeolite suspension dropwise and adsorbed by the zeolite particles. After 6 h, the particles were recovered, dried, and heated at a heating rate of 2 °C min^{-1} to 500 °C for 2 h. After being cooled to room temperature, the products were submitted to a tube furnace and heated to 350 at 2 °C min^{-1} under a flowing stream of 5% H_2 in N_2 for 4 h. Particles of dark brown color were formed.

2.4. Synthesis of Rhodamine-Hydrazine. Rhodamine B (1.20 g, 2.5 mmol) was dissolved in 30 mL ethanol. 3.0 mL (excess) hydrazine hydrate (85%) was then added, dropwise with vigorous stirring at room temperature. After the addition, the stirred mixture was heated to reflux in an air bath for 2 h. The solution changed from dark purple to light orange and became transparent. Then, the mixture was cooled and the solvent was removed under reduced pressure. 1 M HCl was added to the solid in the flask to generate a transparent red solution. After that, 1 M NaOH was added, slowly with stirring until the pH of the solution reached 9−10. The resulting precipitate was filtered and washed 3 times with water, and then vacuum-dried at 100 °C.

2.5. Synthesis of Magnetic Functionalized Zeolite Epoxy Silicon (MMZE). The purified magnetic functionalized zeolite (0.3 g) with trimethoxy- [3-(oxiranylmethoxy) propyl]- silane (0.350 g, 1.5 mmol) in dry toluene (30 mL) was refluxed for 24 h. The product was collected with a magnet and repeatedly washed with toluene, and then vacuum-dried at 100 °C.

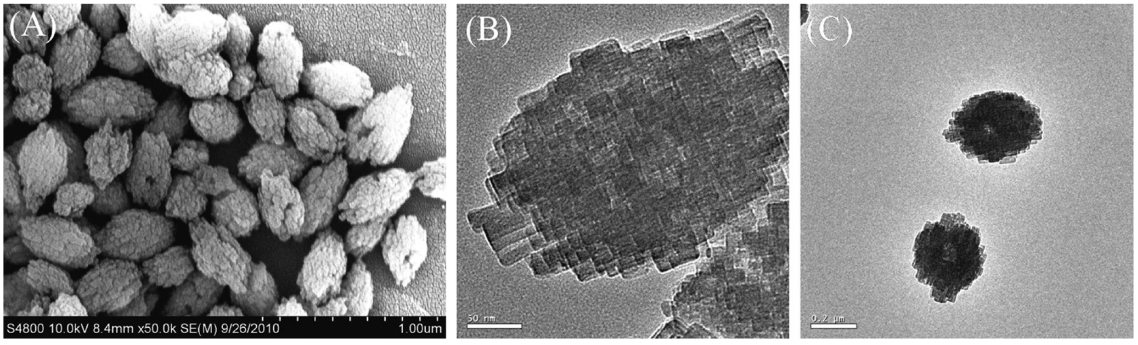

Figure 1. Images of mesoporous self-assembly zeolite clusters (a) SEM, (b) HRTEM, (c) TEM.

2.6. Synthesis of Multifunctional Zeolite Clusters. MMZE (0.3 g) was allowed to react with RH (0.3 g) in toluene (15 mL) at reflux for 10 h. The product was collected with a magnet and repeatedly washed with toluene and then vacuum-dried at 100 °C. The product was dialyzed to remove the free RH.

2.7. Detection and Removal of Hg^{2+} from South Lake Water Samples. South Lake (Changchun, China) water samples were collected. ICP-MS analysis showed no detectable mercury. Therefore, $Hg(NO_3)_2$ was added to simulate contaminated water. For Hg^{2+} detection and removal, the water samples were transferred into SiO_2 tubes (500 μL), and the zeolite-based sensors were added. After separation by magnetic field, the supernatant solutions were collected for ICP-MS analysis.

3. RESULTS AND DISCUSSION

The concept of using nanozeolites as building blocks in the assembly of hierarchical zeolitic materials requires a synthesis method that favors high nucleation rates.[18] This was achieved via highly concentrated gels that were processed using the hydrothermal method. By tuning the reaction mixture (specifically the SiO_2/Al_2O_3, the H_2O/Al_2O_3, and the K_2O/Al_2O_3 ratio), temperature and time, the well structured self-assembled mesoscale zeolite L clusters were successfully obtained. The morphology and structure of the novel materials were analyzed by scanning electron microscopy (SEM) and transmission electron microscopy (TEM) and the textural properties of the materials were determined by N_2 adsorption experiments. The well monodisperse clusters were homogeneous in sizes of about 400 nm with spindlelike morphologies (Figure 1A). The clusters were agglomerated by highly ordered small zeolite L crystallites, which were about 10 nm in diameter (Figure 1B) and 10−20 nm in length. The mesoporosity of the cluster originated from textural pores which formed through the assembly of small crystallites, leading to the three-dimensional agglomerates. Because of the steric hindrance effect, a big hollow pore formed among the stacking zeolites, which could be seen in Figure 1C. To further confirm the structure, we performed wide-angle XRD pattern (Figure 2A). The widening peak of the zeolite L phase suggested that the particle size of zeolite L was in the nanometer level, indicating that the mesoscale clusters were assemblied by small zeolite L clusters.[30]

The nitrogen adsorption/desorption isotherms of MZ showed a typical IV structure with a Brunauer−Emmett−Teller (BET) surface area of 361 $m^2\ g^{-1}$ and pore volume of 0.32 $cm^3\ g^{-1}$ (Figure 2B). The specific surface area was calculated from adsorption data in the relative pressure at P/P_o of 0.30. The total pore volume and pore size distribution were assessed from the amount of nitrogen adsorbed at a relative pressure P/P_o of 0.97. Strikingly, the isotherm showed a strong increase at higher relative pressures, indicating large textural mesoporosity. Similar to sorption in a bed of nanoparticles, a large hysteresis in these zeolite L grains between the adsorption and desorption branch was observed. It could be regarded as a type H1 hysteresis, which was only found in well-defined cylindrical pores or in material agglomerates consisting of extremely uniform particles.[31] The pore size analysis for adsorption data, based on the Barrett−Joyner−Halenda (BJH) pore size distributions, clearly demonstrated that the prepared mesoporous zeolite possessed a mesopores with an average diameter of 3.5 nm. Judging from pore sizes and basal spacing of the zeolite, the peak located around 3.5 nm should be corresponded to the pores formed by the ordered assembly of zeolites. The nitrogen adsorption−desorption isotherms

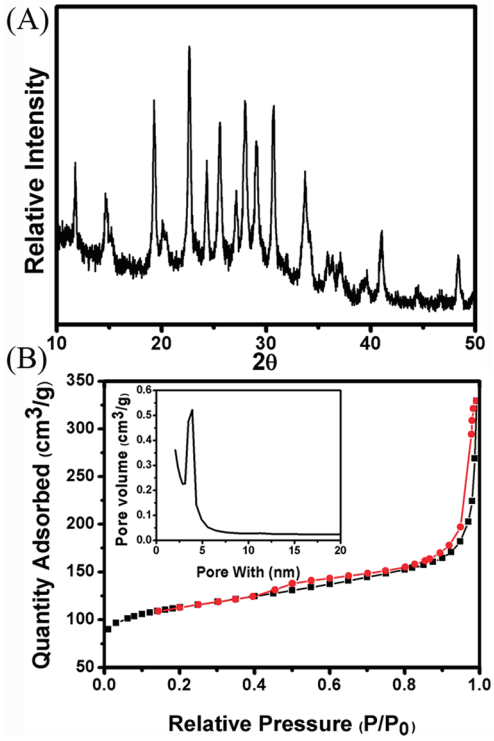

Figure 2. Wide-angle XRD patterns of (A) mesoporous zeolite nanoparticles and (B) the N_2 adsorption−desorption isotherms; adsorption points are marked by black line and desorption points are marked by black line, respectively. Inset is the mesopore size distribution curve.

results also confirmed that MZ could be facilely prepared via the present hydrothermal method.

Adding magnetic property to zeolite composites would enable effective separation of the spent composites from complex multiphase systems by the application of an external magnetic field, opening the door for sorbent regeneration, safe disposal of the waste and/or recovery of loaded valuable species. Research efforts to render zeolites magnetic were still limited. Transition metal ions such as Fe^{3+}, Co^{2+}, and Ni^{2+} had been introduced into zeolites by ion exchange.[32−34] Thermal decomposition of polynuclear iron complex in the Faujasite-type zeolite (NaY) had been reported.[35] However, the reduced metal clusters were not protected and readily oxidized, which limited the application of zeolite to a wider range of systems. Thanks to the large volume mesopores in the zeolite network, superparamagnetic iron oxide nanoparticles could be embedded into the caves by combining the thermal-decomposition and the thermal-reduction, which endowed the as-prepared nanostructures facile manipulation upon an assistant magnetic field. To ensure that the iron oxide nanoparticles were mainly inside the porous network of MMZ, we adopted a two-solvent system to prepare the composite material in our work.[36] MZ was suspended in a nonpolar solvent (n-hexane in our case), and the iron precursor $Fe(NO_3)_3$ was dissolved in a small amount of a polar solvent (acetonitrile), which must be immiscible with the other solvent. When the $Fe(NO_3)_3$ solution was added to the MZ suspension, $Fe(NO_3)_3$ would be adsorbed inside the porous network of MZ. After adsorption of $Fe(NO_3)_3$ onto the MZ, the composite was heated to 500 °C, and MZ-Fe_2O_3 was formed after thermal decomposition. To improve the magnetization at low magnetic field, we

dx.doi.org/10.1021/am201516q | ACS Appl. Mater. Interfaces 2012, 4, 431−437

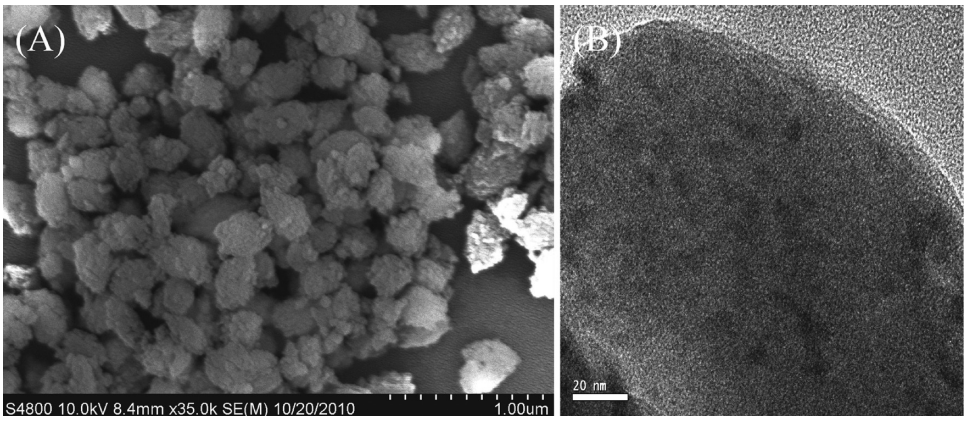

Figure 3. (A) SEM and (B) TEM of the Fe_3O_4 functionalized mesoporous zeolite clusters.

reduced the MZ-Fe_2O_3 by 10% H_2 in argon at 350 °C for 4 h to convert to Fe_3O_4.

SEM and TEM were used to elucidate the nanoscale morphology of the Fe_3O_4 infiltrated zeolitic material. From the SEM image of the MMZ (Figure 3A), we could observe that the prepared magnetite consists of mesoporous clusters had no aggregate after immobilizing the Fe_3O_4 nanocrystals with the same spindle-like morphologies. The formation of iron oxide particles was further confirmed by TEM measurements (Figure 3B). The small dark patches with several nanometers, which could be seen in TEM, consisted of Fe_3O_4 particles. Though some Fe_3O_4 particles were covered at the surface, the mesoporous could be used to enhance the loading capability of Fe_3O_4. Figure 4A showed a representative XRD pattern of the MMZ composite materials after magnetic functionalized. Compared with the XRD patterns of MZ, all the diffraction peaks of zeolite L were present, indicating that the structure of the mother zeolite remained intact after the incorporation of Fe_3O_4 nanoparticles. Because of the functionalization by Fe_3O_4, the intensity was decreased.

After Fe_3O_4 nanocrystal immobilization, the N_2 adsorption/desorption isotherms (Figure 4B) indicated that the surface area and pore volume decreased to 161 $m^2\ g^{-1}$ and 0.27 $cm^3\ g^{-1}$ respectively. The specific surface area was calculated from adsorption data in the relative pressure at P/P_o of 0.30, and the total pore volume and pore size distribution were assessed from the amount of nitrogen adsorbed at a relative pressure P/Po of 0.98. Compared with MZ, there was no significant change in the N_2 adsorption/desorption isotherms, which indicated that the functionalization had not altered the mesopore nature. Although stacked pores seem to be partially blocked by Fe_3O_4 nanocrystals, the BJH pore volume of 0.27 $cm^3\ g^{-1}$ illuminated that the high internal volume was available for the biomolecules adsorption and drug storage. The magnetic property of the MMZ was then studied using a superconducting quantum interference device (SQUID) magnetometer. Figure 5 showed the hysteresis loop of the sample at 300 K. This magnetic mesoporous material was superparamagnetic at room temperature, reaching a saturation moment of 28.3 emu g^{-1}. This magnetic property would allow the nanoparticles to be used for magnetic target or removal applications because they undergo

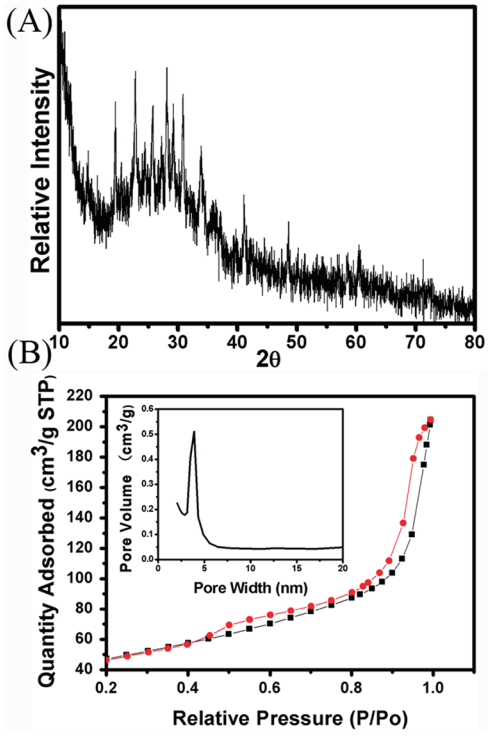

Figure 4. Wide-angle XRD patterns of (A) Fe_3O_4 functionalized mesoporous zeolite nanoparticles and (B) the N_2 adsorption–desorption isotherms, adsorption points are marked by black line and desorption points are marked by black line, respectively. Inset is the mesopore size distribution curve.

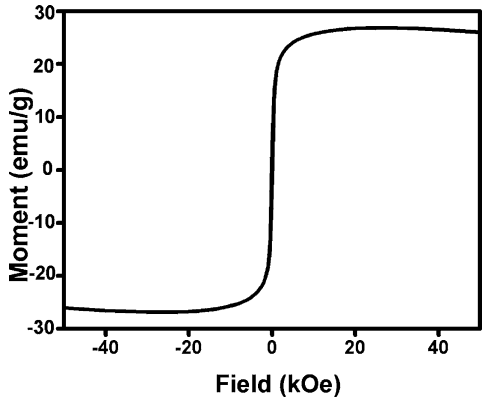

Figure 5. Magnetic hysteresis loops of Fe_3O_4 functionalized mesoporous zeolite nanoparticles.

dx.doi.org/10.1021/am201516q | ACS Appl. Mater. Interfaces 2012, 4, 431–437

strong magnetization, allowing for efficient magnetic separation under an applied external magnetic field.

Recently, various chemosensors for Hg^{2+} have been developed that have the advantages of simplicity, real-time analysis, and good sensitivity.[37−40] In this work, rhodamine-hydrazine (RH) was selected as a signal-transducing unit because of its absorption and emission in the visible region with high excitation coefficients, high fluorescent quantum yield, and high photostability.[37−40] As described in Scheme 1, the MMZ was coated with silica shell using trimethoxy-[3-(oxiranylmethoxy)propyl]-silane (TMOPS) as a silica source in toluene to yield epoxy silicon. Then RH was covalently attached to the surface of multifunctiornal magnetic MMZ. The product was dialyzed to remove the free RH. The incorporation of the epoxy silicon RH moieties into the synthesized magnetic mesoporous microspheres was proved by FTIR and TGA (Figure 6). The band observed at around 1385 and 1518 cm^{-1}

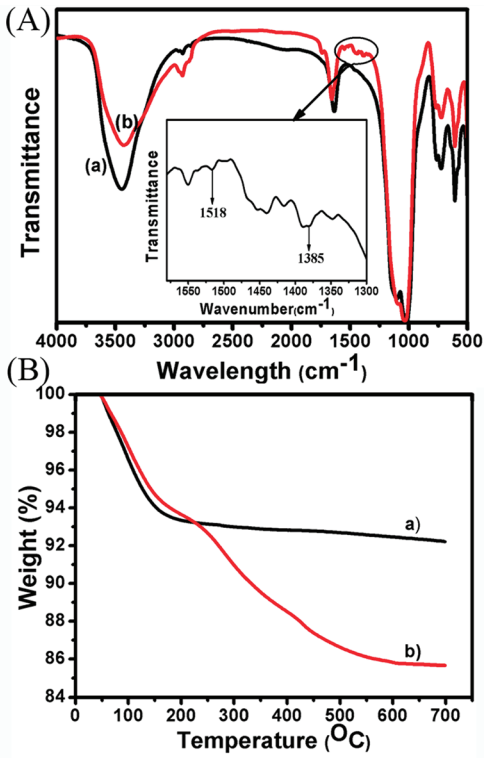

Figure 6. (A) FTIR spectra of the samples (a) Fe_3O_4-zeolite nanoparticles, black, and (b) Fe_3O_4-zeolite-RH, red; (B) TGA of (a) Fe_3O_4-zeolite nanoparticles, black, and (b) Fe_3O_4-zeolite-RH nanoparticles, red.

could be attributed to the stretching vibration of the grafted −C−O-C- group and the bending vibration of σN−H, which indicated the covalent linking of RH. This result was strongly supported by the values obtained from thermogravimetric analysis. As shown in Figure 6B, the mass loss below 200 °C could be attributed to the evaporation of adsorbed water. The TGA platform of Fe_3O_4-zeolite nanoparticles was 92.3%. In contrast to epoxy silica functionalized material, RH decorated material had a sharp weight loss between 200 and 600 °C, indicating that the RH had been removed. The platform of Fe_3O_4-zeolite-RH was 85.7%, confirming that about 6.6 wt % RH was incorporated on zeolite.

Spectroscopic measurements were performed in MeCN/H_2O (1:1, v/v). RH was virtually nonfluorescent in its apo state, which resulted from the efficient photoinduced electron transfer (PET) quenching of the fluorophore by the lone pair of electrons on the nitrogen atom in the benzoyl moiety.[39] After the addition of Hg^{2+}, the fluorescence intensity at 575 nm increased dramatically following excitation at 540 nm due to the delocalized xanthenes moiety of the rhodamine group (Figure 7A). Along with the increase of the Hg^{2+} concentration,

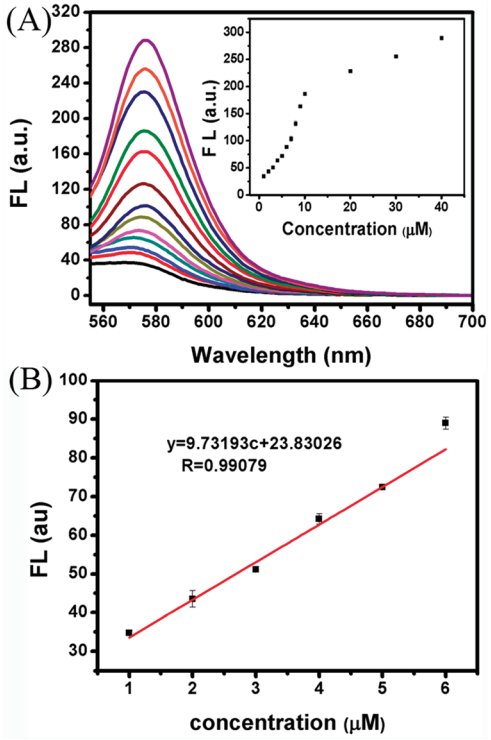

Figure 7. (A) Fluorescence spectra of Fe_3O_4-zeolite-RH nanoparticles (0.02 g L^{-1}) with addition of various concentrations of $Hg(NO_3)_2$ 0, 1, 2, 3, 4, 5, 6, 7, 8, 9, 10, 20, 30, and 40 μM, respectively, in MeCN/H_2O (1:1, v/v) with an excitation at 540 nm. The inset is the fluorescence titration profile. (B) Linear calibration plot for Hg^{2+} in low concentration. The fluorescence intensity was measured at an excitation wavelength of 540 nm, and monitored at a wavelength of 575 nm.

the fluorescence intensity at 575 nm was gradually increased (Figure 7A inset). The limit of detection (LOD) was calculate by the equation LOD = $3S_0/S$, where 3 was the factor at the 99% confidence level, S_0 was the standard deviation of the blank measurements (n = 10), and S was the slope of the calibration curve. The detection limit was determined as low as 3.2×10^{-7} M (Figure 7B). Compared with the free dye, though the sensitivity was adversely affected by the strongly Hg^{2+} adsorption of zeolite, our probe could realize not only detection but also removal of Hg^{2+} ions simultaneously. To additionally evaluate the utility of Z-RH as an ion-selective fluorescence probe for Hg^{2+}, we investigated the competition-based fluorescence emission changes of Z-RH, upon addition of various biologically and environmentally relevant metal ions such as Zn^{2+}, Cu^{2+}, Ca^{2+}, Mn^{2+}, Mg^{2+}, K^+, Cr^{2+}, Na^+, Ni^{2+}, Pb^{2+}, Cd^{2+}, and Fe^{3+} (Figure 8). The fluorescence intensities of MMZ-RH showed no significant changes in the presence of these ions, indicating the sensor had high selectivity for Hg^{2+}.

dx.doi.org/10.1021/am201516q | ACS Appl. Mater. Interfaces 2012, 4, 431−437

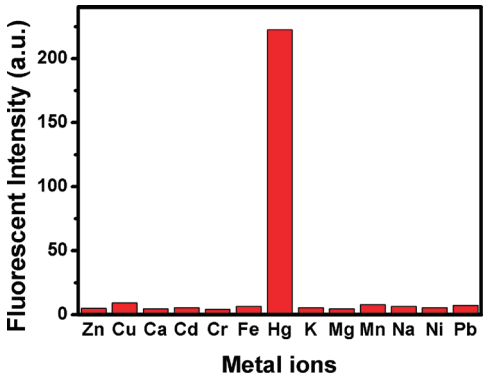

Figure 8. Fluorescence intensity changes of Fe_3O_4-zeolite nanoparticles (0.02 g L^{-1}) in the presence of various ions (10 μM) in MeCN/H_2O (1:1, v/v) with an excitation at 540 nm.

The unique hierarchical mesoporous feature along with the magnetic property promote us to evaluate whether the RH modified MMZ was capable of detecting and removing Hg^{2+} from environmental water samples. Samples from South Lake (a big lake in Changchun, China) were tested. Because no Hg^{2+} contained in these samples as determined by inductively coupled plasma mass spectrometry (ICP-MS), Hg^{2+} was deliberately added to simulate contaminated water. The test samples were prepared by the addition of MMZ-RH (5 mg) to 30 mL of wastewater, containing 6.14 μM Hg^{2+}. Then a small magnet was used to remove the Hg^{2+}-bound MMZ-RH from the water. The amount of Hg^{2+} separated by the magnetic zeolite nanoparticles was determined by ICP-MS. The results indicated that only 5% residual Hg^{2+} remained in wastewater, suggesting that 95% of Hg^{2+} could be removed. Thus, these results clearly demonstrated that our MMZ-RH was capable of detecting and rapidly removing Hg^{2+} from environmental water samples.

4. CONCLUSIONS

In summary, we had demonstrated a simple one-step strategy to fabricate a hierarchical mesoporous zeolite nanocomposite using small zeolite L as building "bricks". Importantly, by taking advantage of the large mesoporous volume, we successfully encapsulated superparamagnetic iron oxide nanocrystals into the mesoporous zeolite network to allow the efficient removal from the analyte solution by using an external magnetic field. It was expected that the encapsulation could be extended to other nanoparticles, such as fluorescent nanocrystals as well as multiple components to further facilitate separation and detection. In addition, by covalent coupling of fluorescent receptor, the combination of well-defined inorganic nanomaterials and organic receptors could play a pivotal role in recognizing, adsorbing, and removing Hg^{2+} with high sensitivity and selectivity. Our approach might lead to the synthesis of a new generation of multifunctional zeolite nanomaterial and could extend the application of zeolite to a much wider range of systems in the field of heterogeneous catalysts, biology, biomedicine, bioanalysis, toxicology, and environmental research.

AUTHOR INFORMATION

Corresponding Author

*Tel: +86 0431 8526 2625. Fax: +86 0431 85262625. E-mail: jren@ciac.jl.cn.

ACKNOWLEDGMENTS

Financial support was provided by the National Basic Research Program of China (Grant 2011CB936004) and National Natural Science Foundation of China (Grants 20831003, 90813001, 20833006, 90913007 and 21072182).

REFERENCES

(1) Mohan, D.; Pittman, C. U. *J. Hazard. Mater.* **2007**, *142*, 1−53.
(2) Ouki, S. K.; Kavannagh, M. *Waste Manage. Res.* **1997**, *15*, 383−394.
(3) Curkovic, L.; Cerjan-Stefanovic, S.; Filipan, T. *Water. Res.* **1997**, *31*, 1379−1382.
(4) Carneiro, C. E. A.; Santana, H. D.; Casado, C.; Coronas, J.; Zaia, D. A. M. *Astrobiology* **2011**, *11*, 409−418.
(5) Kang, Y. J.; Shan, W.; Wu, J. Y.; Zhang, Y. H.; Wang, X. Y.; Yang, W. L.; Tang, Y. *Chem. Mater.* **2006**, *18*, 1861−1866.
(6) Zhang, Y. H.; Wang, X. Y.; Shan, W.; Wu, B. Y.; Fan, H. Z.; Yu, X. J.; Tang, Y.; Yang, P. Y. *Angew. Chem., Int. Ed.* **2005**, *44*, 615−617.
(7) Hu, Y. Y.; Zhang, Y. H.; Ren, N.; Tang, Y. *J. Phys. Chem. C.* **2009**, *113*, 18040−18046.
(8) Kehr, N. S.; Riehemann, K.; El-Gindi, J.; Schäfer, A.; Fuchs, H.; Galla, H. J.; Cola, L. D. *Adv. Funct. Mater.* **2010**, *20*, 2248−2254.
(9) Popovi, Z.; Otter, M.; Calzaferri, G.; Cola, L. D. *Angew. Chem., Int. Ed.* **2007**, *46*, 6188−6191.
(10) Tao, Y.; Kanoh, H.; Abrams, L.; Kaneko, K. *Chem. Rev.* **2006**, *106*, 896−910.
(11) Pavel, C. C.; Schmidt, W. *Chem. Commun.* **2006**, 882−884.
(12) Verboekend, D.; Pérez-Ramírez, J. *Chem.−Eur. J.* **2011**, *17*, 1137−1147.
(13) Liu, Y.; Zhang, W.; Pinnavaia, T. J. *Angew. Chem., Int. Ed.* **2001**, *40*, 1255−1258.
(14) Zhang, Z.; Han, Y.; Zhu, L.; Wang, R. W.; Yu, Y.; Qiu, S. L.; Zhao, D. Y.; Xiao, F. S. *Angew. Chem., Int. Ed.* **2001**, *40*, 1258−1262.
(15) Liu, Y.; Zhang, W. Z.; Pinnavaia, T. J. *J. Am. Chem. Soc.* **2000**, *122*, 8791−8792.
(16) Park, D. H.; Kim, S. S.; Wang, H.; Pinnavaia, T. J.; Papapetrou, M. C.; Lappas, A. A.; Triantafyllidis, K. S. *Angew. Chem., Int. Ed.* **2009**, *48*, 7645−7648.
(17) Cho, S.; Choi, S. D.; Kim, J. H.; Kim, G. J. *Adv. Funct. Mater.* **2004**, *14*, 49−54.
(18) Möoller, K.; Yilmaz, B.; Jacubinas, R. M.; Müuller, U.; Bein, T. *J. Am. Chem. Soc.* **2011**, *133*, 5284−5295.
(19) Lu, Z. D.; Ye, M. M.; Li, N.; Zhong, W. W.; Yin, Y. D. *Angew. Chem., Int. Ed.* **2010**, *49*, 1862−1866.
(20) Kim, H. J.; Lee, S. J.; Park, S. Y.; Jung, J. H.; Kim, J. S. *Adv. Mater.* **2008**, *20*, 3229−3234.
(21) Lee, H. Y.; Bae, D. R.; Park, J. C.; Song, H.; Han, W. S.; Jung, J. H. *Angew. Chem., Int. Ed.* **2009**, *48*, 1239−1243.
(22) Esser-Kahn, A. P.; Iavarone, A. T.; Francis, M. B. *J. Am. Chem. Soc.* **2008**, *130*, 15820−15822.
(23) Wang, C.; Tao, S. Y.; Wei, W.; Meng, C. G.; Liua, F. Y.; Han, M. *J. Mater. Chem.* **2010**, *20*, 4635−4641.
(24) Dave, N.; Chan, M. Y.; Huang, P. J. J.; Smith, B. D.; Liu, J. W. *J. Am. Chem. Soc.* **2010**, *132*, 12668−12673.
(25) Ros-Lis, J. V.; Casasús, R.; Comes, M.; Coll, C.; Marcos, M. D.; Martínez-Máñez, R.; Sancenón, F.; Soto, J.; Amorós, P.; Haskouri, J. E.; Garró, N.; Rurack, K. *Chem.−Eur. J.* **2008**, *14*, 8267−8278.
(26) Zhang, X. Y.; Wang, Q. C.; Zhang, S. Q.; Sun, X. J.; Zhang, Z. S. *J. Hazard. Mater.* **2009**, *168*, 1575−1580.
(27) Sarkar, K.; Dhara, K.; Nandi, M.; Roy, P.; Bhaumik, A.; Banerjee, P. *Adv. Funct. Mater.* **2009**, *19*, 223−234.
(28) Tchounwou, P. B.; Ayensu, W. K.; Ninashvili, N.; Sutton, D. E. V. *Toxicol* **2003**, *18*, 149−175.
(29) Nolan, E. M.; Lippard, S. J. *Chem. Rev.* **2008**, *108*, 3443−3480.
(30) Megelski, S.; Calzaferri, G. *Adv. Funct. Mater.* **2001**, *11*, 277−286.
(31) Thommes, M. *Ser. Chem. Eng.* **2004**, *4*, 317−364.

(32) Lu, A. H.; Nitz, J. J.; Comotti, M.; Weidenthaler, C.; Schlichte, K.; Lehmann, C. W.; Terasaki, O.; Schüth, F. *J. Am. Chem. Soc.* **2010**, *132*, 14152−14162.
(33) Kato, M.; Ikeda, T.; Kodaira, T.; Takahashi, S. *Microporous Mesoporous Mater.* **2011**, *142*, 444−453.
(34) de Souza, M. O. D.; Mendes, F. M. T.; de Souza, R. F.; dos Santos, J. H. Z. *Microporous Mesoporous Mater.* **2004**, *69*, 217−221.
(35) Dutta, B.; Jana, S.; Bhattacharjee, A.; Gütlich, P.; Iijima, S. I.; Koner, S. *Inorg. Chim. Acta* **2010**, *363*, 696−704.
(36) Yiu, H. H. P.; Niu, H. J.; Biermans, E.; Tendeloo, G. V.; Rosseinsky, M. J. *Adv. Funct. Mater.* **2010**, *20*, 1599−1609.
(37) Suresh, M.; Shrivastav, A.; Mishra, S.; Suresh, E.; Das, A. *Org. Let.* **2008**, *10*, 3013−3016.
(38) Kim, H. N.; Lee, M. H.; Kim, H. J.; Kim, J. S.; Yoon, J. *Chem. Soc. Rev.* **2008**, *37*, 1465−1472.
(39) Yuan, M. J.; Zhou, W. D.; Liu, X. F.; Zhu, M.; Li, J. B.; Yin, X. D.; Zheng, H. Y.; Zuo, Z. C.; Ouyang, C. B.; Liu, H. B.; Li, Y. L.; Zhu, D. B. *J. Org. Chem.* **2008**, *73*, 5008−5014.
(40) Zheng, H.; Qian, Z. H.; Xu, L.; Yuan, F. F.; Lan, L. D.; Xu, J. G. *Org. Lett.* **2006**, *8*, 859−861.